PROCEEDINGS A

rspa.royalsocietypublishing.org

Research

Cite this article: Li S, Su Y, Li R. 2016 Splitting of the neutral mechanical plane depends on the length of the multi-layer structure of flexible electronics. *Proc. R. Soc. A* **472**: 20160087.
http://dx.doi.org/10.1098/rspa.2016.0087

Received: 5 February 2016
Accepted: 9 May 2016

Subject Areas:
mechanical engineering, mechanics

Keywords:
neutral mechanical plane, multi-layer structure, flexible electronics, structure design

Authors for correspondence:
Yewang Su
e-mail: yewangsu@imech.ac.cn
Rui Li
e-mail: ruili@dlut.edu.cn

THE ROYAL SOCIETY
PUBLISHING

Splitting of the neutral mechanical plane depends on the length of the multi-layer structure of flexible electronics

Shuang Li[1], Yewang Su[1,2,3] and Rui Li[4]

[1]State Key Laboratory of Nonlinear Mechanics, Institute of Mechanics, Chinese Academy of Sciences, Beijing 100190, People's Republic of China
[2]Department of Civil and Environmental Engineering, and
[3]Department of Mechanical Engineering, Northwestern University, Evanston, IL 60208, USA
[4]State Key Laboratory of Structural Analysis for Industrial Equipment, Department of Engineering Mechanics, Dalian University of Technology, Dalian 116024, People's Republic of China

YS, 0000-0002-5961-0490

Multi-layer structures with soft (compliant) interlayers have been widely used in flexible electronics and photonics as an effective design for reducing interactions among the hard (stiff) layers and thus avoiding the premature failure of an entire device. The analytic model for bending of such a structure has not been well established due to its complex mechanical behaviour. Here, we present a rational analytic model, without any parameter fitting, to study the bending of a multi-layer structure on a cylinder, which is often regarded as an important approach to mechanical reliability testing of flexible electronics and photonics. For the first time, our model quantitatively reveals that, as the key for accurate strain control, the splitting of the neutral mechanical plane depends not only on the relative thickness of the middle layer, but also on the length-to-thickness ratio of the multi-layer structure. The model accurately captures the key quantities, including the axial strains in the top and bottom layers, the shear strain in the middle layer and the locations of the neutral mechanical planes of the top and bottom layers. The effects of the length of the multi-layer and the thickness of the middle layer are elaborated. This work is very useful for the design of multi-layer structure-based flexible electronics and photonics.

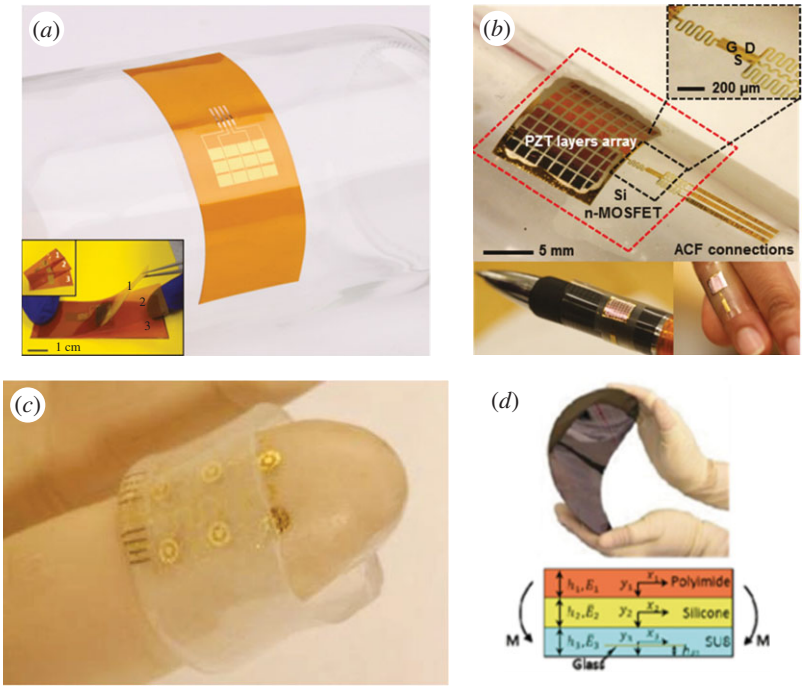

Figure 1. (*a*) Stacking and bending test of three hard PZT-based piezoelectric MEHs. (*b*) Conformable piezoelectric pressure sensor with multi-layer structures. (*c*) Finger-tip electronics with multi-layer structures. (*d*) Flexible glass photonic device with multi-layer structures. (Online version in colour.)

1. Introduction

Multi-layer structures are encountered in various engineering applications such as aerospace vehicles, marine vessels and civil infrastructures. Such structures have been investigated extensively in recent years, focusing on the static and dynamic behaviour, mechanical failure, structural design and manufacture [1–4]. The most popular multi-layer structures are lightweight sandwich panels that are based on two stiff face sheets separated by a soft foam core and that have unique mechanical properties such as high rigidity, high impact energy absorption, stable deformation mode and adaptation to loading conditions. In flexible electronics and photonics, multi-layer structures with both soft (compliant) and hard (stiff) materials are also widely used in order to reduce the strains in the hard layers, which are often composed of functional devices [5–7]. Such applications include flexible piezoelectric mechanical energy harvesters (MEHs) [8] (figure 1*a*), conformable piezoelectric pressure sensors [9] (figure 1*b*), finger-tip electronics [10] (figure 1*c*), flexible glass photonic devices [11] (figure 1*d*), etc. However, incorrect stacking of the layers would cause premature failure of the entire device. Therefore, it is necessary to explore effective designs of the laminated structures so that they can undergo large deformation during fabrication and use.

Recently, a novel local-neutral-axis design (figure 1*d*) was implemented to render the structure highly mechanically flexible, enabling repeated bending of the photonic device down to sub-millimetre bending radii without any measurable degradation in optical performance [11]. This design is also referred to as the splitting of the neutral mechanical plane [8]. It is known that the neutral mechanical plane is a layer within a structure where the material is not under stress, either compression or tension. That is, strain in the neutral mechanical plane is zero when the structure bends. For the design of flexible electronics and photonics, one always expects accurate strain control in the brittle device. Therefore, it is very useful to split the neutral mechanical plane into each hard layer where the brittle device is placed. In this way, the strength of each layer is

reached almost simultaneously. This could avoid premature failure. Some simplified theoretical models were developed to quantitatively study the pure bending and buckling behaviour of the multi-layer structures, where a large modulus mismatch among the different layers is a distinctive feature [8,11–13]. Actually, previous studies simply incorporated the effects of the thickness and elastic modulus, and there have been no discussions on the effects of the length of the structure due to the modelling complexity induced by coupling deformation. However, as illustrated in the following, our finite-element analysis (FEA) reveals that the influence of the length cannot be neglected. Therefore, an accurate mechanics model incorporating the length effect is critically needed to comprehensively grasp the mechanical behaviour, which can provide guidelines for the design of such structures against mechanical failure.

In this paper, we establish an approach to accurate analytic modelling of multi-layers with moduli of very different orders of magnitude (e.g. silicon and polydimethylsiloxane, which have elastic moduli of five orders of magnitude difference), where the classical beam theory [14] with plane cross-sectional assumption fails. A very important application of the model is the characterization of the bendability of the flexible electronics and photonics, in which the key index is the minimum bending radius of the device. This could be realized by attaching the device to cylindrical surfaces with different radii. The index is the minimum cylindrical radius at which the device remains intact. Such a bending test is illustrated in figure 1*a*, where a stack of three hard lead zirconate titanate (PZT)-based piezoelectric MEHs are laminated, with a soft adhesive in between [8], and bent to fit a glass cylinder. For convenience, we focus on the three-layer sandwich structure, which has two hard layers with a soft adhesive in between. The analytic model is established and an accurate solution is obtained to quantitatively capture the structural behaviour as well as to provide guidelines for the refined design of flexible devices against premature failure.

2. The model

Figure 2 shows a three-layer sandwich structure with length $2L$ and thicknesses h_t, h_m and h_b from top to bottom at the natural, stress-free state (figure 2*a*) and the deformed state on a cylinder with radius R (figure 2*b*). Young's moduli and Poisson's ratios for the layers are E_t, E_m and E_b, and v_t, v_m and v_b, respectively. The middle layer is much softer than the other layers and serves as the shear lag whose large shear deformation is the dominant mechanical behaviour. This is the main difference from multi-layers with similar elastic properties. Owing to the symmetry of the structure, only the right half model with length L is considered.

Multi-layer structures for flexible electronics and photonics are generally long and thin [15–18]. Therefore, the thickness change of the layers is neglected. As shown in figure 2, x is the curvilinear coordinate along the central axis of a layer, with the origin O at the axis centre. Let u_t and u_b denote the displacement increments at the central axes of the top and bottom layers during deformation. The corresponding membrane strains (ε_t and ε_b) and bending curvatures (κ_t and κ_b) are

$$\varepsilon_t = \frac{\mathrm{d}u_t}{\mathrm{d}x},\ \kappa_t = \frac{1}{R + h_b + h_m + h_t/2},\ \varepsilon_b = \frac{\mathrm{d}u_b}{\mathrm{d}x} \quad \text{and} \quad \kappa_b = \frac{1}{R + h_b/2}. \tag{2.1}$$

As shown in figure 3, the shear strain of the middle layer, γ_m, is obtained by

$$\begin{aligned}\gamma_m &\approx \frac{\gamma_{m1} + \gamma_{m2}}{2} \approx \frac{\widehat{\mathrm{BC}} + \widehat{\mathrm{AF}}}{2\mathrm{AB}} = \frac{\widehat{\mathrm{BD}} - \widehat{\mathrm{CD}} + \widehat{\mathrm{AE}} - \widehat{\mathrm{EF}}}{2\mathrm{AB}} \\ &= \frac{1}{h_m}\left[\frac{R + h_b + h_m/2}{R + h_b/2}(x + u_b) - \frac{R + h_b + h_m/2}{R + h_b + h_m + h_t/2}(x + u_t)\right].\end{aligned} \tag{2.2}$$

The variational approach [19,20] is used to yield the governing equations in terms of the displacements. The total elastic energy, U, of the right half structure consists of the membrane

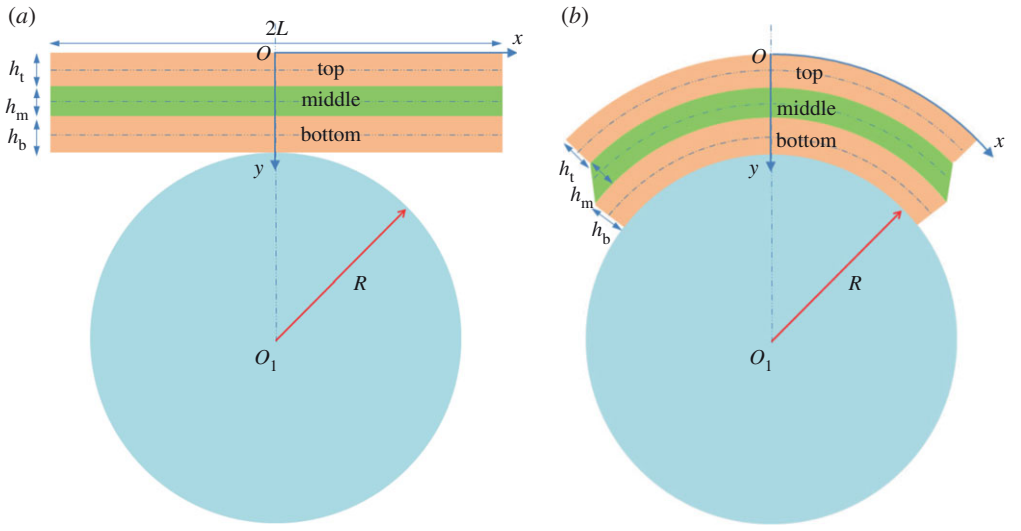

Figure 2. Theoretical model of a three-layer sandwich structure. (*a*) The natural, stress-free state. (*b*) The deformed state on a cylinder. (Online version in colour.)

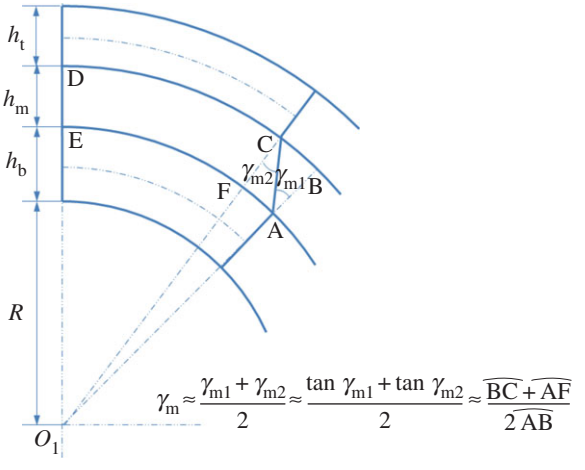

Figure 3. Schematic illustration of the shear strain of the middle layer. (Online version in colour.)

energy and bending energy of the top and bottom layers as well as the shear energy of the middle layer. We have

$$U=\int_0^L\left(\frac{1}{2}\overline{EI}_t\kappa_t^2+\frac{1}{2}\overline{EA}_t\varepsilon_t^2\right)\mathrm{d}x+\int_0^L\left(\frac{1}{2}\overline{EI}_b\kappa_b^2+\frac{1}{2}\overline{EA}_b\varepsilon_b^2\right)\mathrm{d}x+\int_0^L\frac{1}{2}Gh_m\gamma_m^2\,\mathrm{d}x, \tag{2.3}$$

where $\overline{EI}_t=E_th_t^3/[12(1-\nu_t^2)]$, $\overline{EA}_t=E_th_t/(1-\nu_t^2)$ and $\overline{EI}_b=E_bh_b^3/[12(1-\nu_b^2)]$, $\overline{EA}_b=E_bh_b/(1-\nu_b^2)$ are the beam theory-based effective bending stiffnesses and tensile stiffnesses of the top and bottom layers, respectively [21]; $G=E_m/[2\,(1+\nu_m)]$ is the shear modulus of the middle layer.

Substituting equations (2.1) and (2.2) in equation (2.3), we have

$$U = \int_0^L \left[\frac{1}{2}\overline{EI}_t \frac{1}{(R + h_b + h_m + h_t/2)^2} + \frac{1}{2}\overline{EA}_t \left(\frac{du_t}{dx}\right)^2 \right] dx + \int_0^L \left[\frac{1}{2}\overline{EI}_b \frac{1}{(R + h_b/2)^2} + \frac{1}{2}\overline{EA}_b \left(\frac{du_b}{dx}\right)^2 \right] dx + \int_0^L \frac{1}{2} G h_m \left\{ \frac{1}{h_m} \left[\frac{R + h_b + h_m/2}{R + h_b/2}(x + u_b) - \frac{R + h_b + h_m/2}{R + h_b + h_m + h_t/2}(x + u_t) \right] \right\}^2 dx. \tag{2.4}$$

Variation of equation (2.4) $\delta U = 0$ gives the governing equations

$$\left.\begin{aligned} &\frac{d^2 u_t}{dx^2} - \frac{aG}{\overline{EA}_t h_m}[(a-b)x + (au_t - bu_b)] = 0 \\ \text{and} \quad &\frac{d^2 u_b}{dx^2} + \frac{bG}{\overline{EA}_b h_m}[(a-b)x + (au_t - bu_b)] = 0, \end{aligned}\right\} \tag{2.5}$$

and the boundary conditions

$$\left.\begin{aligned} &u_t(0) = 0, \quad u_b(0) = 0 \\ \text{and} \quad &\frac{du_t(L)}{dx} = 0, \quad \frac{du_b(L)}{dx} = 0, \end{aligned}\right\} \tag{2.6}$$

where $a = (R + h_b + h_m/2)/(R + h_b + h_m + h_t/2)$ and $b = (R + h_b + h_m/2)/(R + h_b/2)$. Equation (2.6) implies that there is no axial displacement at the plane of symmetry and no axial strain at the right-hand end of the top and bottom layers.

The general solution of equation (2.5) is

$$\left.\begin{aligned} u_t = &-\frac{ac}{b}(C_1 + C_2)\cosh\left[\sqrt{d(b^2 + ca^2)}\frac{x}{h_m}\right] - \frac{ac}{b}(C_1 - C_2)\sinh\left[\sqrt{d(b^2 + ca^2)}\frac{x}{h_m}\right] \\ &+ \left[\frac{b}{a}(C_3 + 1) - 1\right]x + \frac{b}{a}C_4 \\ \text{and} \quad u_b = &(C_1 + C_2)\cosh\left[\sqrt{d(b^2 + ca^2)}\frac{x}{h_m}\right] + (C_1 - C_2)\sinh\left[\sqrt{d(b^2 + ca^2)}\frac{x}{h_m}\right] + C_3 x + C_4, \end{aligned}\right\} \tag{2.7}$$

where $c = E_b h_b(1 - \nu_t^2)/[E_t h_t(1 - \nu_b^2)]$ and $d = Gh_m(1 - \nu_b^2)/(E_b h_b)$. The constants C_1–C_4 are determined by substituting equation (2.7) into equation (2.6), which yields

$$\left.\begin{aligned} C_1 &= -\frac{b(a-b)}{b^2 + ca^2} \frac{h_m}{\sqrt{d(b^2 + ca^2)}\cosh\left[\sqrt{d(b^2 + ca^2)}(L/h_m)\right]}, \\ C_2 &= \frac{b(a-b)}{b^2 + ca^2} \frac{h_m}{\sqrt{d(b^2 + ca^2)}\cosh\left[\sqrt{d(b^2 + ca^2)}(L/h_m)\right]}, \\ C_3 &= \frac{b(a-b)}{b^2 + ca^2} \\ \text{and} \quad C_4 &= 0. \end{aligned}\right\} \tag{2.8}$$

Thus u_t and u_b are obtained as

$$\left.\begin{aligned} u_t &= \frac{ac(a-b)}{b^2+ca^2}\left\{\frac{\sinh\left[\sqrt{d(b^2+ca^2)}(x/h_m)\right]}{\sqrt{d(b^2+ca^2)}\cosh\left[\sqrt{d(b^2+ca^2)}(L/h_m)\right]}h_m - x\right\} \\ \text{and}\quad u_b &= \frac{b(a-b)}{b^2+ca^2}\left\{x - \frac{\sinh\left[\sqrt{d(b^2+ca^2)}(x/h_m)\right]}{\sqrt{d(b^2+ca^2)}\cosh\left[\sqrt{d(b^2+ca^2)}(L/h_m)\right]}h_m\right\}. \end{aligned}\right\} \tag{2.9}$$

Substituting equation (2.9) into equations (2.1) and (2.2), we obtain the membrane strains of the top and bottom layers as well as the shear strain of the middle layer,

$$\left.\begin{aligned} \varepsilon_t &= \frac{ac(a-b)}{b^2+ca^2}\left\{\frac{\cosh\left[\sqrt{d(b^2+ca^2)}(x/h_m)\right]}{\cosh\left[\sqrt{d(b^2+ca^2)}(L/h_m)\right]} - 1\right\}, \\ \varepsilon_b &= \frac{b(a-b)}{b^2+ca^2}\left\{1 - \frac{\cosh\left[\sqrt{d(b^2+ca^2)}(x/h_m)\right]}{\cosh\left[\sqrt{d(b^2+ca^2)}(L/h_m)\right]}\right\} \\ \text{and}\quad \gamma_m &= \frac{(b-a)\sinh\left[\sqrt{d(b^2+ca^2)}(x/h_m)\right]}{\sqrt{d(b^2+ca^2)}\cosh\left[\sqrt{d(b^2+ca^2)}(L/h_m)\right]}. \end{aligned}\right\} \tag{2.10}$$

The mode of deformation for the top and bottom layers is that of the slender beam because they are hard, long and thin; this model is known as the Euler–Bernoulli beam, where the axial strains are linearly distributed [22]. This yields

$$\varepsilon = \begin{cases} \varepsilon_t - \kappa_t\left(y - \dfrac{h_t}{2}\right) & \\ \quad = \dfrac{ac(a-b)}{b^2+ca^2}\left\{\dfrac{\cosh\left[\sqrt{d(b^2+ca^2)}(x/h_m)\right]}{\cosh\left[\sqrt{d(b^2+ca^2)}(L/h_m)\right]} - 1\right\} & \\ \quad - \dfrac{y - h_t/2}{R + h_b + h_m + h_t/2} & \text{for } 0 \le y \le h_t, \\ \varepsilon_b - \kappa_b\left(y - h_t - h_m - \dfrac{h_b}{2}\right) & \\ \quad = \dfrac{b(a-b)}{b^2+ca^2}\left\{1 - \dfrac{\cosh\left[\sqrt{d(b^2+ca^2)}(x/h_m)\right]}{\cosh\left[\sqrt{d(b^2+ca^2)}(L/h_m)\right]}\right\} & \\ \quad - \dfrac{y - h_t - h_m - h_b/2}{R + h_b/2} & \text{for } h_t + h_m \le y \le h_m + h_t + h_b, \end{cases} \tag{2.11}$$

where y is the distance in the normal direction from the top surface of the multi-layers. The locations of the neutral mechanical planes of the top and bottom layers, y_t and y_b, are determined by equating to zero the strains in equation (2.11), by which we have

$$\left.\begin{aligned} y_t &= \frac{c(a-b)(R+h_b+h_m/2)}{b^2+ca^2}\left\{\frac{\cosh\left[\sqrt{d(b^2+ca^2)}(x/h_m)\right]}{\cosh\left[\sqrt{d(b^2+ca^2)}(L/h_m)\right]} - 1\right\} + \frac{h_t}{2} \\ \text{and}\quad y_b &= \frac{(a-b)(R+h_b+h_m/2)}{b^2+ca^2}\left\{1 - \frac{\cosh\left[\sqrt{d(b^2+ca^2)}(x/h_m)\right]}{\cosh\left[\sqrt{d(b^2+ca^2)}(L/h_m)\right]}\right\} + h_t + h_m + \frac{h_b}{2}. \end{aligned}\right\} \tag{2.12}$$

For simplification, we now focus on the case in which $E_t = E_b = E$, $h_t = h_b = h$ and $v_t = v_b = v_m = v$. We have

$$a = \frac{R + h(1 + \bar{h}_m/2)}{R + h(3/2 + \bar{h}_m)}, \quad b = \frac{R + h(1 + \bar{h}_m/2)}{R + h/2}, \quad c = 1 \quad \text{and} \quad d = \frac{E_m \bar{h}_m (1 - v)}{2E}, \tag{2.13}$$

where $\bar{h}_m = h_m/h$. The membrane strains of the top and bottom layers as well as the shear strain of the middle layer become

$$\left.\begin{aligned} \varepsilon_t &= \frac{a(a-b)}{a^2+b^2}\left\{\frac{\cosh\left[\sqrt{d(a^2+b^2)}(\rho\bar{x}/\bar{h}_m)\right]}{\cosh\left[\sqrt{d(a^2+b^2)}(\rho/\bar{h}_m)\right]} - 1\right\}, \\ \varepsilon_b &= \frac{b(a-b)}{a^2+b^2}\left\{1 - \frac{\cosh\left[\sqrt{d(a^2+b^2)}(\rho\bar{x}/\bar{h}_m)\right]}{\cosh\left[\sqrt{d(a^2+b^2)}(\rho/\bar{h}_m)\right]}\right\} \\ \text{and} \quad \gamma_m &= \frac{(b-a)\sinh\left[\sqrt{d(a^2+b^2)}(\rho\bar{x}/\bar{h}_m)\right]}{\sqrt{d(a^2+b^2)}\cosh\left[\sqrt{d(a^2+b^2)}(\rho/\bar{h}_m)\right]}, \end{aligned}\right\} \tag{2.14}$$

where $\rho = L/h$ and $\bar{x} = x/L$. The normalized locations of the neutral mechanical planes of the top and bottom layers are

$$\left.\begin{aligned} \bar{y}_t &= \frac{y_t}{h} = \frac{b(a-b)}{a^2+b^2}\left(\frac{R}{h} + \frac{1}{2}\right)\left\{\frac{\cosh\left[\sqrt{d(a^2+b^2)}(\rho\bar{x}/\bar{h}_m)\right]}{\cosh\left[\sqrt{d(a^2+b^2)}(\rho/\bar{h}_m)\right]} - 1\right\} + \frac{1}{2} \\ \text{and} \quad \bar{y}_b &= \frac{y_b}{h} = \frac{b(a-b)}{a^2+b^2}\left(\frac{R}{h} + \frac{1}{2}\right)\left\{1 - \frac{\cosh\left[\sqrt{d(a^2+b^2)}(\rho\bar{x}/\bar{h}_m)\right]}{\cosh\left[\sqrt{d(a^2+b^2)}(\rho/\bar{h}_m)\right]}\right\} + \bar{h}_m + \frac{3}{2}. \end{aligned}\right\} \tag{2.15}$$

3. Results and discussion

A typical multi-layer structure with the geometric parameters and mechanical properties $R = 0.014$ m, $h = 10^{-5}$ m, $E = 1000$ MPa, $E_m = 100$ KPa and $v = 0.4$ is examined. The membrane strains in both the top and bottom layers are plotted in figure 4 for $\bar{h}_m = 1$ and $\rho = 100$, 200, 400, 1000 (figure 4*a*), and for $\rho = 100$ and $\bar{h}_m = 0.5$, 1, 2 (figure 4*b*). Excellent agreement is observed between our analytic model and the FEA results (see appendix A for details of the FEA modelling). As shown in figure 4*a*, the membrane strain is approximately linearly distributed in the hard layers for a relatively short structure with small ρ and approaches the constant for a relatively long structure with large ρ except around the end of the structure. The membrane strain increases with an increase of ρ (figure 4*a*) and decreases with $\bar{h}_m$ (figure 4*b*). This indicates that the thick middle layer and the short multi-layer structure help to reduce the membrane strains in the hard layers.

Figure 5 shows the shear strain distribution in the soft middle layer for $\bar{h}_m = 1$ and $\rho = 100$, 200, 400, 1000 (figure 5*a*), and for $\bar{h}_m = 0.5$, 1, 2 and $\rho = 100$ (figure 5*b*) and 1000 (figure 5*c*). FEA perfectly validates the analytic results. At a given $\bar{h}_m$, the longer multi-layer structure helps to reduce the shear strain around $\bar{x} = 0$ (figure 5*a*). It is interesting to observe that the shear strain decreases with an increase of $\bar{h}_m$ for a relatively short structure (figure 5*b*), but increases with $\bar{h}_m$ around $\bar{x} = 0$ for a relatively long structure (figure 5*c*). In general, a thick middle layer and a short multi-layer structure help to increase the shear strain in most of the middle layer, which benefits the transfer of strain energy to the middle layer such that the strains in the hard layers diminish.

The normalized locations of the neutral mechanical planes are plotted in figure 6 for $\bar{h}_m = 1$ and $\rho = 100$, 200, 400, 1000 (figure 6*a*), and for $\rho = 100$ and $\bar{h}_m = 0.5$, 1, 2 (figure 6*b*). The analytic

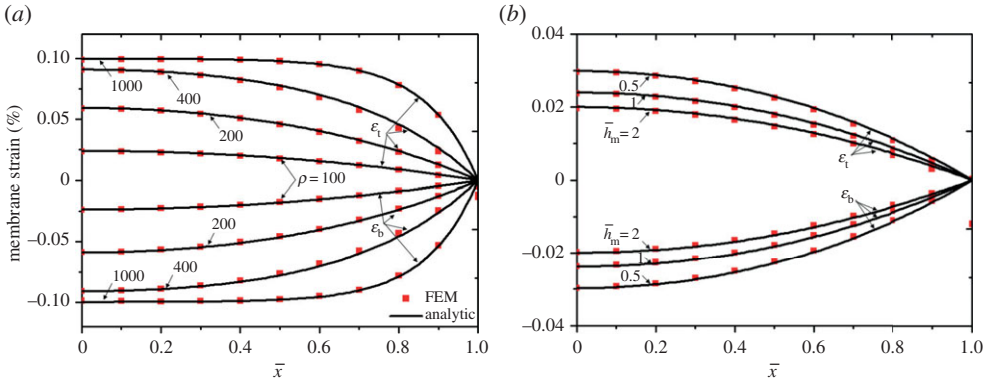

Figure 4. Membrane strain distribution in both the top and bottom layers for (*a*) $\bar{h}_m = 1$ and (*b*) $\rho = 100$. (Online version in colour.)

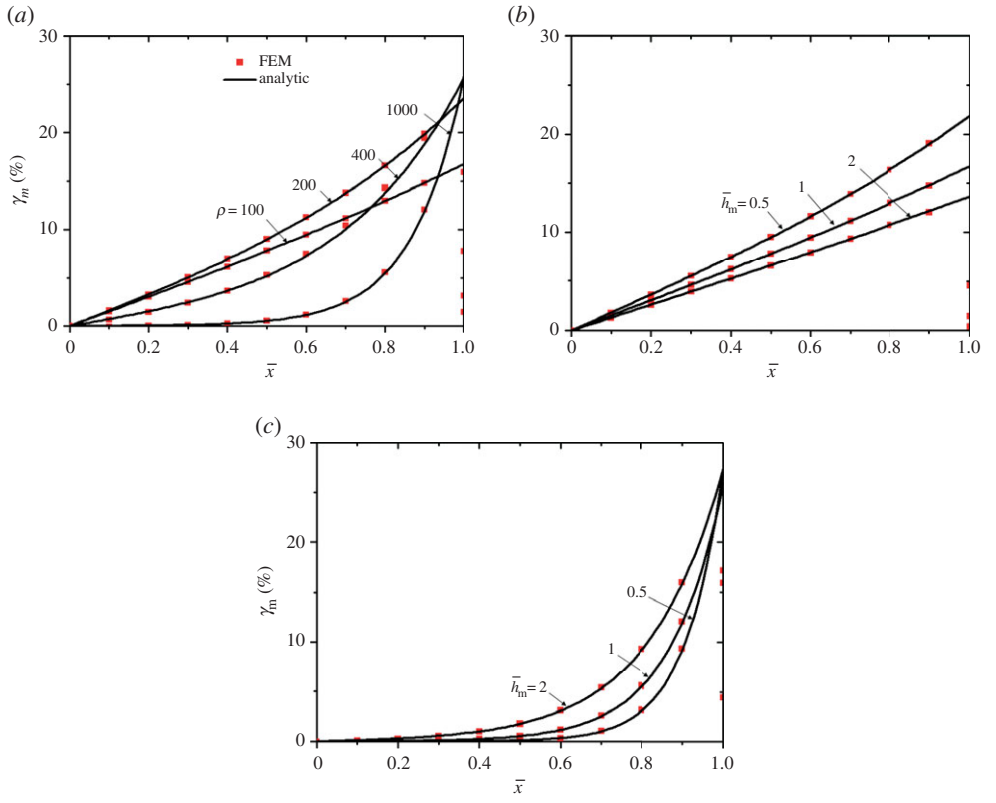

Figure 5. Shear strain distribution in the middle layer for (*a*) $\bar{h}_m = 1$, (*b*) $\rho = 100$ and (*c*) $\rho = 1000$. (Online version in colour.)

solutions agree very well with FEA. It is seen that the neutral mechanical planes shift towards the centre of the hard layers with decreasing ρ and with increasing $\bar{h}_m$, which implies that a short and thick adhesive helps to split the neutral mechanical plane and thus could avoid premature failure of the entire device.

A meaningful discussion of the extreme cases from equation (2.15) is helpful in the design of the multi-layer structure. (i) The middle layer is soft enough such that $E_m \to 0$ and thus $d \to 0$. In this case, $\bar{y}_t \to 1/2$ and $\bar{y}_b \to \bar{h}_m + 3/2$, which means that both the top and bottom layers bend

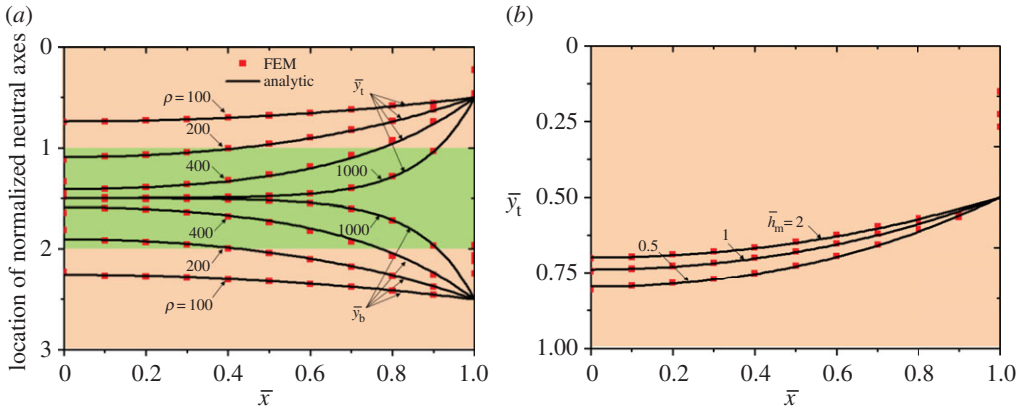

Figure 6. Normalized locations of the neutral mechanical planes in (*a*) the top and bottom layers for $\bar{h}_m = 1$ and in (*b*) the top layer for $\rho = 100$. (Online version in colour.)

as independent single layers and splitting of the neutral mechanical plane is achieved. (ii) The middle layer is hard enough such that $E_m \to \infty$ and thus $d \to \infty$. In this case, $\bar{y}_t \to (1/2)\,\bar{h}_m + 1$ and $\bar{y}_b \to (1/2)\bar{h}_m + 1$ for $R \gg h$ and h_m, which means that the plane section holds for the entire multi-layer structure and there is only one neutral mechanical plane. (iii) The length of the structure is much larger than its thickness such that $\rho \to \infty$. In this case, the result is the same as that in case (ii). (iv) The length of the structure is much smaller than its thickness such that $\rho \to 0$. In this case, the result is the same as that in case (i). (v) The thickness of the middle layer is much smaller than that of the top and bottom layers such that $h_m \to 0$. In this case, the result is the same as that in case (ii).

It should be noted that, taking $y = 0$ and $h_m + h_t + h_b$ in equation (2.11), respectively, the axial strains at the top and bottom surfaces of the multi-layers are readily obtained:

$$\left.\begin{aligned}\varepsilon_{\text{top surface}} &= \frac{ac(a-b)}{b^2+ca^2}\left\{\frac{\cosh\left[\sqrt{d(b^2+ca^2)}(x/h_m)\right]}{\cosh\left[\sqrt{d(b^2+ca^2)}(L/h_m)\right]}-1\right\}+\frac{h_t/2}{R+h_b+h_m+h_t/2}\\ \text{and}\quad \varepsilon_{\text{bottom surface}} &= \frac{b(a-b)}{b^2+ca^2}\left\{1-\frac{\cosh\left[\sqrt{d(b^2+ca^2)}(x/h_m)\right]}{\cosh\left[\sqrt{d(b^2+ca^2)}(L/h_m)\right]}\right\}-\frac{h_b/2}{R+h_b/2}.\end{aligned}\right\} \tag{3.1}$$

This is very useful to rapidly predict the extreme strains in the structure.

4. Conclusion

In summary, we have established a sufficiently accurate, FEA-validated analytic model for cylindrical bending of a multi-layer structure with soft interlayers for flexible electronics and photonics, in which we incorporate the length effect, for the first time, in depicting the mechanical behaviour of such structures. The axial strains in the top and bottom layers as well as the shear strain in the middle layer are analytically obtained and the locations of the neutral mechanical planes of the top and bottom layers are pinpointed. We analyse a typical multi-layer structure in detail to reveal the effects of the normalized length of the multi-layers and normalized thickness of the middle layer. In general, a short and thick adhesive helps to split the neutral mechanical plane and thus can avoid the premature failure of the entire device. It should be noted that the three-layer sandwich structure is adopted for demonstration and similar structures with more layers can be analysed with the same method, which will yield the same conclusion. The work

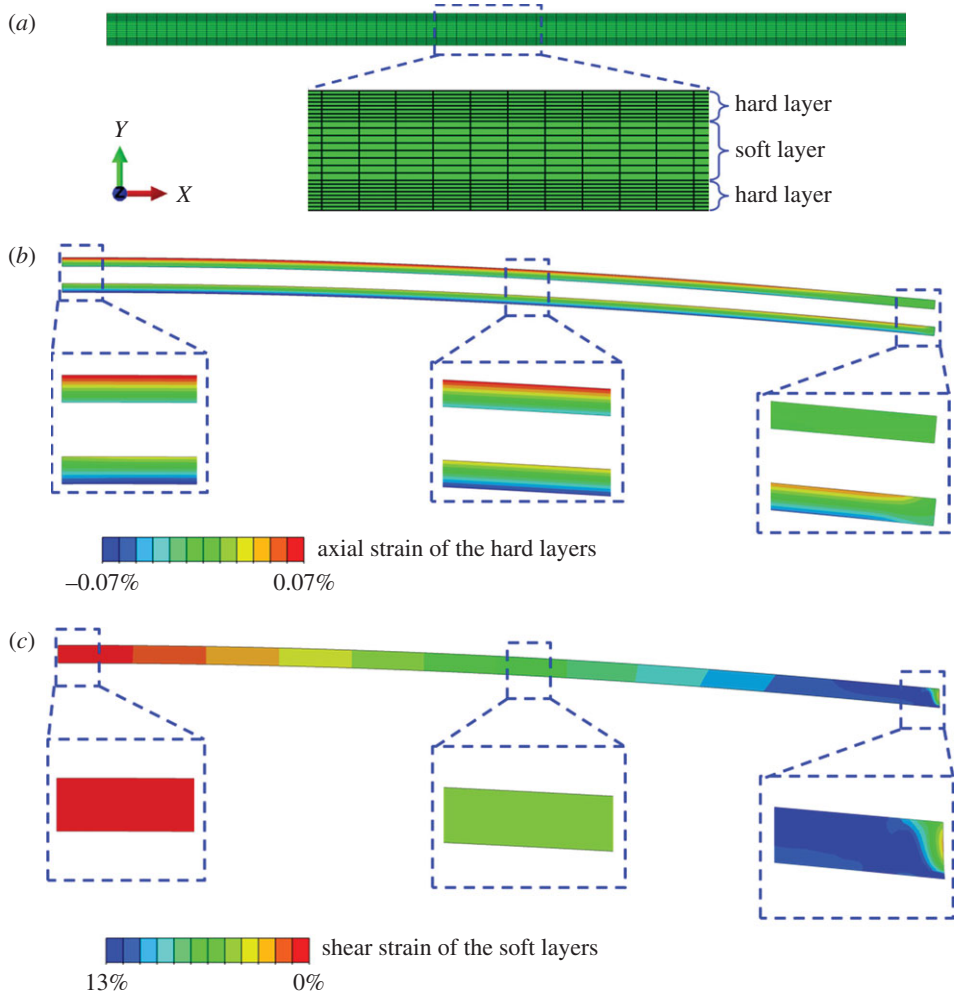

Figure 7. The finite-element meshes and strain distribution of the model ($\bar{h}_m = 2$, $\rho = 100$). (*a*) The mesh of the multi-layers. (*b*) The axial strain distribution of the hard layers. (*c*) The shear strain distribution of the soft layer. (Online version in colour.)

in this paper is expected to serve as a benchmark model for designing multi-layers with very different elastic properties.

Authors' contributions. All authors conceived the idea of this work, performed the theoretical analysis and the numerical simulation, wrote the manuscript and gave final approval for publication.

Competing interests. The authors declare no competing financial interests.

Funding. Y.S. and R.L. acknowledge support from the National Natural Science Foundation of China (grant nos 11572323 and 11302038). Y.S. also acknowledges support from the Chinese Academy of Sciences via the 'Hundred Talent program'.

Appendix A. Finite-element analysis modelling

FEA modelling using the ABAQUS software package was conducted to validate the analytic results of equations (2.12) and (2.13). The bottom surface of the three-dimensional sandwich structure was attached to an extremely hard three-dimensional shell without friction or delamination. The shell was bent to realize the bending of the multi-layers. With the same length and thickness as those in the analytic model for the multi-layers, the symmetric boundary

condition was imposed on the FEA model and only the right half was analysed. The displacement along the width direction was restricted to realize the plane strain state. The displacement along the length direction was restricted on the left-hand side of the multi-layers while the left-hand side of the shell was clamped. In-plane rotation with angle L/R was imposed on the right-hand side of the shell. Without any assumption of plane section or shear lag, the 20-node quadratic brick element C3D20R was employed for the multi-layer structure and the 8-node doubly curved thick shell element S8R was adopted for the shell. As an example, figure 7*a* shows the finite-element meshes of all of the multi-layers for $\bar{h}_m = 2$ and $\rho = 100$. The numbers of uniform grids for each layer are 80 in the length direction (x), eight in the thickness direction (y), and one in the width direction (z). Figure 7*b*,*c* shows the axial strain and shear strain distribution, respectively.

References

1. Allen HG. 1969 *Analysis and design of structural sandwich panels*. Oxford, UK: Pergamon Press.
2. Zhu F, Zhao L, Lu G, Wang Z. 2008 Deformation and failure of blast-loaded metallic sandwich panels—experimental investigations. *Int. J. Impact Eng.* **35**, 937–951. (doi:10.1016/j.ijimpeng.2007.11.003)
3. Li R, Kardomateas GA. 2008 Nonlinear high-order core theory for sandwich plates with orthotropic phases. *AIAA J.* **46**, 2926–2934. (doi:10.2514/1.37430)
4. Hohe J, Librescu L, Oh SY. 2006 Dynamic buckling of flat and curved sandwich panels with transversely compressible core. *Compos. Struct.* **74**, 10–24. (doi:10.1016/j.compstruct.2005.03.003)
5. Kim D-H, Lu N, Huang Y, Rogers JA. 2012 Materials for stretchable electronics in bioinspired and biointegrated devices. *MRS Bull.* **37**, 226–235. (doi:10.1557/mrs.2012.36)
6. Rogers JA, Someya T, Huang Y. 2010 Materials and mechanics for stretchable electronics. *Science* **327**, 1603–1607. (doi:10.1126/science.1182383)
7. Kim D-H, Xiao J, Song J, Huang Y, Rogers JA. 2010 Stretchable, curvilinear electronics based on inorganic materials. *Adv. Mater.* **22**, 2108–2124. (doi:10.1002/adma.200902927)
8. Su Y, Li S, Li R, Dagdeviren C. 2015 Splitting of neutral mechanical plane of conformal, multilayer piezoelectric mechanical energy harvester. *Appl. Phys. Lett.* **107**, 041905. (doi:10.1063/1.4927677)
9. Dagdeviren C *et al*. 2014 Conformable amplified lead zirconate titanate sensors with enhanced piezoelectric response for cutaneous pressure monitoring. *Nat. Commun.* **5**, 4496. (doi:10.1038/ncomms5496)
10. Su Y, Li R, Cheng H, Ying M, Bonifas AP, Hwang K-C, Rogers JA, Huang Y. 2013 Mechanics of finger-tip electronics. *J. Appl. Phys.* **114**, 164511. (doi:10.1063/1.4828476)
11. Li L, Lin H, Qiao S, Zou Y, Danto S, Richardson K, Musgraves JD, Lu N, Hu J. 2014 Integrated flexible chalcogenide glass photonic devices. *Nat. Photonics* **8**, 643–649. (doi:10.1038/nphoton.2014.138)
12. Shi Y, Rogers JA, Gao C, Huang Y. 2014 Multiple neutral axes in bending of a multiple-layer beam with extremely different elastic properties. *Trans. ASME, J. Appl. Mech.* **81**, 114501. (doi:10.1115/1.4028465)
13. Lu N, Yang S, Qiao S. 2014 Mechanics of flexible electronics and photonics based on inorganic micro- and nanomaterials. In *Micro- and nanotechnology sensors, systems, and applications VI* (eds T George, MS Islam, AK Dutta). Proceedings of SPIE, vol. 9083. Bellingham, WA: SPIE.
14. Timoshenko S. 1930 *Strength of materials*. New York, NY: D. Van Nostrand Company.
15. Lee YC, Liu TS. 2014 Deformation of multilayer flexible electronics subjected to torque. *Exp. Tech.* **38**, 13–20. (doi:10.1111/j.1747-1567.2011.00780.x)
16. Lin KL, Jain K. 2009 Design and fabrication of stretchable multilayer self-aligned interconnects for flexible electronics and large-area sensor arrays using excimer laser photoablation. *IEEE Electron Devices Lett.* **30**, 14–17. (doi:10.1109/LED.2008.2008665)
17. Yu S, Zhang W, Li L, Xu D, Dong H, Jin Y. 2013 Transparent conductive Sb-doped SnO_2/Ag multilayer films fabricated by magnetron sputtering for flexible electronics. *Acta Mater.* **61**, 5429–5436. (doi:10.1016/j.actamat.2013.05.031)
18. Zheng J, Tucker MB, Teng L. 2011 Failure mechanics of organic-inorganic multilayer permeation barriers in flexible electronics. *Compos. Sci. Technol.* **71**, 365–372. (doi:10.1016/j.compscitech.2010.12.003)

19. Ekeland I. 1974 Variational principle. *J. Math. Anal. Appl.* **47**, 324–353. (doi:10.1016/0022-247X(74)90025-0)
20. Seliger RL, Whitham GB. 1968 Variational principles in continuum mechanics. *Proc. R. Soc. Lond. A* **305**, 1–25. (doi:10.1098/rspa.1968.0103)
21. Almeida PAD, Ferreira CAT. 1998 Determination of the effective bending stiffness of nailed laminated wood beams. In *Proc. 5th World Conf. on Timber Engineering, Montreux, Switzerland, 17–20 August 1998*, vol. 1, pp. 425–431. Lausanne, Switzerland: Presses Polytechniques et universitaires romandes.
22. Timoshenko S. 1953 *History of strength of materials*. New York, NY: McGraw-Hill Company.